Rapid Communications

Experimental evidence for selection rules in multiphoton double ionization of helium and neon

K. Henrichs,[1] S. Eckart,[1] A. Hartung,[1] D. Trabert,[1] J. Rist,[1] H. Sann,[1] M. Pitzer,[2] M. Richter,[1] H. Kang,[1,3] M. S. Schöffler,[1] M. Kunitski,[1] T. Jahnke,[1] and R. Dörner[1,*]

[1]*Institut für Kernphysik, J. W. Goethe-Universität, Max-von-Laue-Strasse 1, 60438 Frankfurt am Main, Germany*

[2]*Institut für Physik, Universität Kassel, Heinrich-Plett-Strasse 40, 34132 Kassel, Germany*

[3]*State Key Laboratory of Magnetic Resonance and Atomic and Molecular Physics, Wuhan Institute of Physics and Mathematics, Chinese Academy of Sciences, Wuhan 430071, China*

(Received 22 November 2017; revised manuscript received 6 February 2018; published 27 March 2018)

We report on the observation of a multipeak structure in the correlated two-electron energy distribution from strong-field double ionization of helium using laser pulses with a wavelength of 394 nm and an intensity of 3×10^{14} W/cm^2. For selected regions of electron emission angles the peaks emerging at energies corresponding to an odd number of absorbed photons are suppressed. We interpret this as direct results of quantum-mechanical selection rules. For neon these features occur for even photon numbers. By that we attribute this effect to the parity of the continuum wave function. A comparison with analogous data for single-photon double ionization is given.

DOI: 10.1103/PhysRevA.97.031405

The ionization of atoms by an electromagnetic wave has been studied across a tremendous range of light intensities and wavelengths. Our physical picture of the interaction process changes completely from the perturbative single-photon regime considered by Einstein over the multiphoton to the tunneling regime accessible today with tabletop lasers and free-electron laser sources. Despite the very different interaction mechanisms, there are still several quantum features, which are expected to be universal across these different intensity and wavelength regimes. The most obvious one is the quantization of energy transfer from the field to the ejected electron(s). Along with this energy quantization more subtle features are predicted to be quantized, such as the change in parity and angular momentum between the bound initial and the final states of the fragments (electrons and ion). The transfer of one quantum of energy, i.e., the absorption of one photon, is accompanied by a parity change between the initial and the final states. It is also, within the dipole approximation, accompanied by the transfer of one quantum of angular momentum.

Energy quantization is easily observed in the case of *single ionization* in the different intensity regimes: For one-photon processes it is the basis for spectroscopy. For multiphoton processes in the intensity regime of 10^{13}–10^{14} W/cm^2 it produces a comb of discrete structures in the energy spectrum of the emitted electron spaced by the photon's energy. These structures are commonly described as above-threshold-ionization (ATI) peaks, referring to the fact that more photons can be absorbed than needed to overcome the ionization threshold. For *double ionization* the quantized excess energy can be shared between the electrons, but the energy quantization can still be observed in the sum energy of both electrons [1] and is used accordingly for spectroscopy in the one-photon case as well [2,3]. In double ionization in the multiphoton strong-field regime the discretization of the electron's sum energy ($E_1 + E_2$) leads to above-threshold-double-ionization (ATDI) peaks at energies given by

$$E_1 + E_2 = nh\nu - I_{p1} - I_{p2} - 2U_p. \quad (1)$$

where $I_{p1,2}$ refers to the first- and the second-ionization potentials of the atom and U_p to the ponderomotive energy. The latter is defined in atomic units as $U_p = I/2c\omega^2_{\mathrm{Laser}}$ (c being the speed of light, ω_{Laser} being the laser frequency, and I being the laser intensity). n refers to the number of absorbed photons. Although Eq. (1) has been confirmed by many calculations [4–10], most strong-field double-ionization experiments failed to resolve such discrete structures, presumably due to the variation of U_p across the laser focus (see Ref. [11] for the only experimental confirmation).

The consequences of parity and angular momentum transfer to the two-electron continuum has been first worked out in detail for the single-photon case [12]. They lead to selection rules, which are observable as nodes in the differential cross section occurring for certain emission angles and energy sharings of both electrons if they are measured in coincidence (see Ref. [13] for a generalization). In the single-photon regime these theoretical predictions have been confirmed also experimentally in detail, e.g.. for the double ionization of helium [14], neon [15], and H_2 [16,17]. These selection rules have been generalized for absorption of more than one photon by Ni *et al.* [18]. They have formulated two rules, which hold for double ionization of an even initial state and an odd number of absorbed photons. For the special case of the double ionization of helium the two-body momentum space covered by the first selection rule is a subset of the one covered by selection rule S_2:

(1) (S_1) Back-to-back emission of electrons with equal energy ($k_1 = k_2$): $\vec{k}_1 = -\vec{k}_2$ is forbidden (the red dashed line in Fig. 1).

*doerner@atom.uni-frankfurt.de

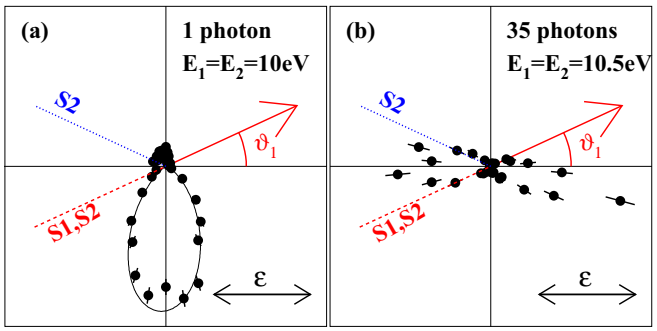

FIG. 1. Joint angular distributions and selection rules for the double ionization of helium (double-ionization potential 79 eV). (a) Absorption of one linearly polarized photon ($h\nu = 99$ eV, synchrotron radiation, and the reanalysis of data from experiment reported in Ref. [26]). Both electrons share the excess energy equally, electron 1 was selected at a $20^\circ < \vartheta_1 < 30^\circ$ angle (the red arrow) with respect to the polarization axis ϵ (the horizontal line). The angular distribution of the second electron measured in coincidence is plotted for electrons on the plane of the paper ($\pm 25^\circ$). The full line shows a parametrization of the cross section (equation on p. 5154 of Ref. [26]). The angles blocked by selection rules S_1 and S_2 are shown by the red dashed and blue dotted lines. (b) The same geometry as (a) but for the case of the absorption of 35 photons ($h\nu = 3.2$ eV, 3×10^{14} W/cm^2, 45 fs). Only electrons of equal energy which occurred at energies depicted by the circle in Fig. 2 are plotted.

(2) (S_2) The emission of electrons of equal energy with angles $\vartheta_1 + \vartheta_2 = 180^\circ$ is forbidden (the blue dotted and red dashed lines in Fig. 1).

Both rules result from the Pauli principle, the parity, and total angular momentum of the two-body state. Accordingly, these selection rules do not depend on the physical mechanism of emission: They hold true for shake-off as well as knock-off [19], for sequential as well as nonsequential ionization, and for the regime of tunnel ionization as well as for three (five, and so on) photon transitions from a free-electron laser. In all quantum-mechanical calculations, these selection rules are implicitly implemented (see, e.g., in direct solutions of the time-dependent Schrödinger equation [4,7,20], S-matrix calculations [21,22], or close-coupling methods [23]). The only experimental hint was reported in experimental work on two-photon double ionization where the selection rules do not apply. There doubly charged helium ions with zero momentum were observed, which are suppressed by the selection rules in the one-photon case [24,25].

In Fig. 1 we illustrate the joint electron angular distributions for the cases of double ionization by one photon of 99 eV (reanalysis of the dataset presented in Ref. [26]) and the corresponding case of the absorption of 35 photons of 32 eV at 3×10^{14} W/cm^2 from our current experiment. The physical mechanisms leading to double ionization in both cases are completely different. Accordingly, these differences manifest themselves in vastly differing angular distributions. After absorption of a single photon the electrons evolve freely, and the angular distribution obtained at 20-eV excess energy is shaped by the joint action of electron repulsion and the influence of the selection rules which effectively blocks an extended range of angles (see Ref. [14] for details). As only one unit of angular momentum is absorbed from the field also the individual electrons have comparably low angular momenta, and the angular distribution shows no narrow peaks. In the strong-field multiphoton case, on the contrary, much higher angular momenta are present allowing for narrow features in the angular distributions to form. The sharply directed electron emission along the polarization axis of the laser light is caused by the strong electric field of the laser, which drives the electrons along this direction. The nodes expected due to the selection rules are supposed to appear at the angles indicated by the dashed lines. Obviously, these are practically impossible to observe on these extremely narrow angular distributions. We therefore pursued the following route in order to achieve the goal of providing the missing experimental evidence for the selection rules in strong-field physics: Instead of selecting a subset of data corresponding to a fixed even or odd number of absorbed photons from the total dataset and inspecting the angular distributions (as performed in Fig. 1), we rather select ranges of emission angles for both electrons which are either suppressed or permitted by the selection rules and then inspect the electron sum energy spectrum (1). By inspecting this sum energy histogram we can investigate whether the absorption of an even or odd number of photons is present or suppressed.

In our experiment, we used linearly polarized light at a wavelength of 394 nm ($\hbar\nu \approx 3.2$ eV) and employed a cold target recoil-ion momentum spectroscopy reaction microscope [27] for the coincidence detection of all charged particles. A Ti:sapphire laser system (Wyvern-500, KMLabs, 45 fs, 100 kHz) at a central wavelength of 778 nm was used to generate the second harmonic at 394 nm with a 200-μm β-barium borate crystal. We determined the intensity of the resulting 394-nm pulses to be 3×10^{14} W/cm^2 *in situ* by the ponderomotive shift of the sum energy of the electron and proton after dissociative ionization of H_2. The calibration of U_p (≈ 4.5 eV) has been verified by examining the energies of the ATI peaks of helium single ionization during the whole experiment (approximately 140 h of data acquisition). From this we estimated the accuracy of our intensity calibration to be better than $\pm 20\%$. The laser pulses were focused onto a supersonic gas jet target by a spherical mirror ($f = 60$ mm). Electrons and ions were guided by a parallel electric (1.6 V/cm) and magnetic field (6.3 G) towards two position- and time-sensitive multichannel plate detectors with three-layer delay line anodes for the position readout [28]. The measurement was conducted at a count rate of 5-kHz ions and 15-kHz electrons. We used a 5-μm nozzle and piezocontrolled collimators in order to adjust the width of the gas jet to be much smaller than the laser's Rayleigh length. We found a ratio of $He^{2+}/He^{1+} = 3 \times 10^{-4}$ at $3 \pm 0.6 \times 10^{14}$ W/cm^2. The background pressure in the interaction chamber was below 2×10^{-11} mbars, which was essential to reduce the amount of $H_2{}^+$ overlapping in time of flight with the He^{2+} ions.

The dataset recorded contains approximately 70 000 events where two electrons were measured in coincidence with the He^{2+} ion and about a factor of 6 more in which only one of the two electrons was detected. For these events we obtain the momentum of the missing electron from the measured momenta of the ion and the other electron using momentum conservation. In this case about 30% false $H_2{}^+$ coincidences had to be subtracted.

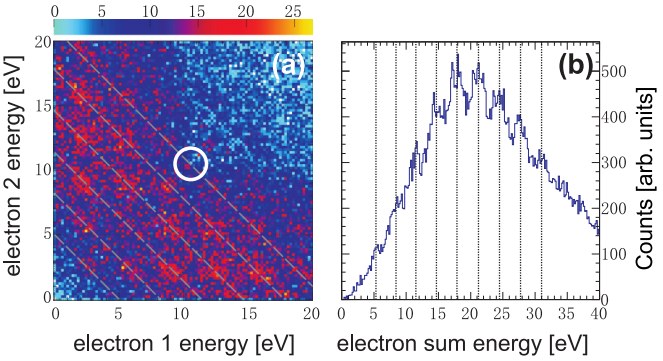

FIG. 2. Energy spectra of *two directly measured* electrons after the double ionization of helium atoms by laser pulses with a peak intensity of 3×10^{14} W/cm^2 and a central wavelength of 394 nm. (a) Joint energy distribution of both electrons (energy of one electron plotted versus energy of the second). The gray diagonal lines indicate constant sum energies at the values calculated using Eq. (1). The white circle at $E_1 = E_2 = 10.5$ eV shows the region of events selected for Fig. 1(b). (b) Sum energy of both electrons [the same data as in (a)]. The vertical lines correspond to the gray lines in (a) indicating the calculated position of the ATDI peaks.

In Fig. 2(b) we show the sum energy of electrons measured in coincidence with a doubly charged He ion. The vertical lines represent the expected peak positions for the independently determined intensity of 3×10^{14} W/cm^2 ($U_p \approx 4.5$ eV) according to Eq. (1). We used the lowest intensity possible to still reach sufficient count rates since for higher intensities the ATDI peaks were not resolvable due to a stronger focal averaging effect. The measured peak positions perfectly match the calculated positions. This is the key to assign a total number of absorbed photons n to each peak in the sum energy spectrum. Additionally, Fig. 2(a) shows the joint energy distribution of both emitted electrons. The gray diagonal lines represent the sum energies depicted by the vertical lines in Fig. 2(b). Along these diagonals distinct peaks occur. Such peaks have already been observed in the correlated energy spectrum in the double ionization of argon [11]. They were attributed to a doubly excited intermediate state. For helium similar peaks along the diagonal ATDI lines have been predicted in Ref. [7] for 800 nm; the physical mechanism producing these peaks for helium remained open in these calculations.

As introduced above, selection rules hold true for all odd numbers of absorbed photons, whereas for even numbers they do not apply [18]. As demonstrated in Fig. 2(a) our experimental results allow for counting how many photons have been absorbed. This prerequisite allows us to observe a possible manifestation of those selection rules in strong-field double ionization. The corresponding results are shown in Fig. 3. In the left (right) column the occurrence of selection rule S_1 (S_2) is examined. Let us first consider S_1. In Fig. 3(b) the sum energy of the emitted electron pair is shown for the subset of double-ionization events where the electrons are emitted approximately back to back (angle α between both electrons is $140^\circ \leqslant \alpha \leqslant 180^\circ$). Every single ATDI peak is observed as depicted by the black arrows in Fig. 3. If we now restrict this dataset to cases where in addition both electrons share the total excess energy equally (the energy difference of both electrons

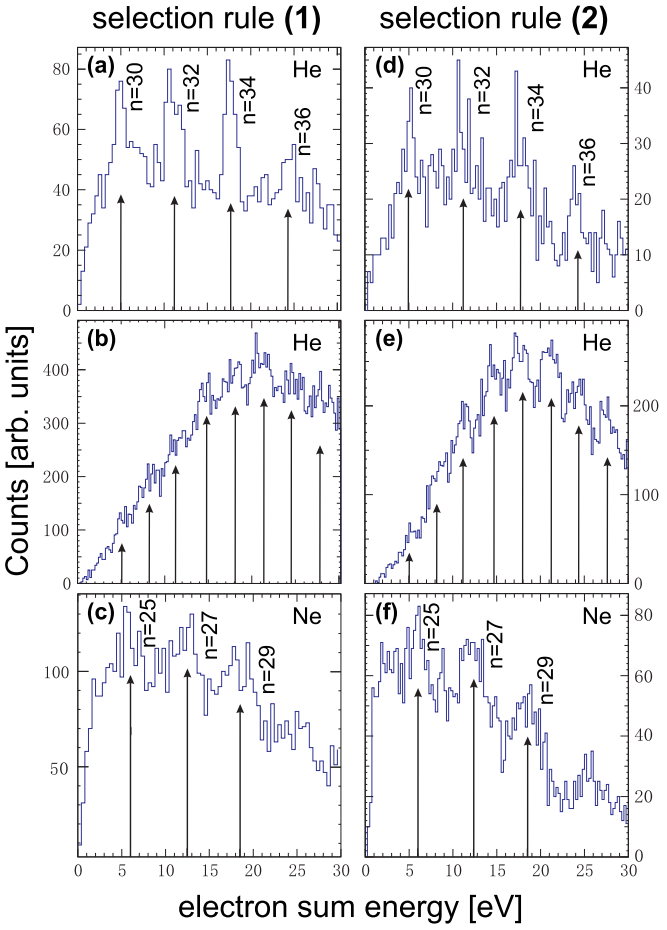

FIG. 3. Demonstration of the consequences of quantum-mechanical selection rules in the double ionization of helium and neon. Left column: Selection rule S_1 (see the text), which forbids $\vec{k}_1 = \vec{k}_2$. The sum energy is plotted for all events with $140^\circ < \alpha < 180^\circ$ (α is the angle between the two electrons) and (a) and (c) equal energy sharing and (b) no equal energy sharing condition. In (a) and (c) equal energy sharing is fulfilled if the energy of both electrons differs by less than 1 eV. Right column: Selection rule S_2 (see the text), which does not allow emission with $\vartheta_1 + \vartheta_2 = 180^\circ$ for an equal energy sharing. The sum energy is plotted for $130^\circ \leqslant \vartheta_1 + \vartheta_2 \leqslant 230^\circ$, [Fig. 2(a)] equal energy sharing, and [Fig. 2(b)] the unequal energy sharing condition. Here, only one electron was measured, and the momentum vector, the kinetic energy, respectively, of the second electron were determined by momentum conservation and the measured ion momentum. The numbers in (a), (c), (d), and (f) correspond to the amount of absorbed photons n. For helium, S_1 and S_2 forbid absorption of an odd number of photons (a) and (d). Due to the opposite parity of the ground state, for neon even numbers of photons are suppressed (c) and (f).

is less than 1 eV), we obtain the histogram shown in panel (a) of Fig. 3. For these events, selection rule (1) applies, and only ATDI peaks with an even number of absorbed photons (labeled by the numbers, respectively) are observed. This is in line with the prediction that for an odd number of absorbed photons no emission within this part of the momentum space is allowed.

The same approach is taken to test selection rule (2) in Figs. 3(d) and 3(e). Here the individual angles ϑ_1, ϑ_2 between the electrons and the polarization axis (i.e., in the laboratory

frame) are now examined. As a reference, the sum energy of all electron pairs fulfilling $130^\circ < \vartheta_1 + \vartheta_2 < 230^\circ$ is plotted in Fig. 3(e). Again, all ATDI peaks are present. That changes if one selects the subset of electrons which fulfill "equal energy sharing" in Fig. 3(d). As for selection rule S_1, also for S_2, only those ATDI peaks survive that are related to an even number of absorbed photons.

To illustrate the general character of the selection rules we show the equivalent data obtained employing neon as a target gas in Figs. 3(c) and 3(f). The ground state (^3P) of Ne^{2+} has the opposite parity as compared to He^{2+}. Consequently, the absorption of odd numbers of photons is suppressed. We cannot resolve the final ionic state but expect the contribution from the second and third excited states (^1D and ^1S) to be significantly smaller as they are 3.2 and 6.9 eV higher in energy.

In conclusion we have shown experimental evidence for two quantum-mechanical selection rules shaping the two-electron continuum in multiphoton double ionization. Our findings show that, despite the great success of classical modeling of strong-field double ionization, details of the process cannot be understood without discussing subtle consequences on the quantum nature of photon-matter interaction. The consequences of the quantum nature of the process are energy quantization (see also Ref. [29] for a molecular case) as well as well-defined parity and angular momentum transfer. This makes double ionization a prominent example highlighting that the quantum entanglement of the electrons in atomic and molecular bound states is not broken by the interaction with a strong laser field, instead this entanglement is projected into the continuum becoming visible as electron-electron correlation in coincidence experiments.

This Rapid Communication was supported by DFG. K.H. and A.H. thank the Studienstiftung des deutschen Volkes for financial support. We thank A. Scrinzi, J. Zhu, V. Majety, U. Thumm, and A. Becker for helpful discussions.

[1] R. Wehlitz, F. Heiser, O. Hemmers, B. Langer, A. Menzel, and U. Becker, Phys. Rev. Lett. **67**, 3764 (1991).
[2] M. Nakano, F. Penent, M. Tashiro, T. P. Grozdanov, M. Žitnik, S. Carniato, P. Selles, L. Andric, P. Lablanquie, J. Palaudoux, E. Shigemasa, H. Iwayama, Y. Hikosaka, K. Soejima, I. H. Suzuki, N. Kouchi, and K. Ito, Phys. Rev. Lett. **110**, 163001 (2013).
[3] J. H. D. Eland, O. Vieuxmaire, T. Kinugawa, P. Lablanquie, R. I. Hall, and F. Penent, Phys. Rev. Lett. **90**, 053003 (2003).
[4] M. Lein, E. K. U. Gross, and V. Engel, Phys. Rev. A **64**, 023406 (2001).
[5] Q. Liao and P. Lu, Phys. Rev. A **82**, 021403 (2010).
[6] J. S. Parker, B. J. S. Doherty, K. T. Taylor, K. D. Schultz, C. I. Blaga, and L. F. DiMauro, Phys. Rev. Lett. **96**, 133001 (2006).
[7] A. Zielinksi, V. P. Majety, and A. Scrinzi, Phys. Rev. A **93**, 023406 (2016).
[8] J. S. Parker, L. R. Moore, K. J. Meharg, D. Dundas, and K. T. Taylor, J. Phys. B: At., Mol. Opt. Phys. **34**, L69 (2001).
[9] G. S. J. Armstrong, J. S. Parker, and K. T. Taylor, New J. Phys. **13**, 013024 (2011).
[10] A. Liu and U. Thumm, Phys. Rev. A **89**, 063423 (2014).
[11] K. Henrichs, M. Waitz, F. Trinter, H. Kim, A. Menssen, H. Gassert, H. Sann, T. Jahnke, J. Wu, M. Pitzer, M. Richter, M. S. Schöffler, M. Kunitski, and R. Dörner, Phys. Rev. Lett. **111**, 113003 (2013).
[12] F. Maulbetsch and J. Briggs, J. Phys. B: At., Mol. Opt. Phys. **28**, 551 (1995).
[13] A. W. Malcherek and J. S. Briggs, J. Phys. B: At., Mol. Opt. Phys. **30**, 4419 (1997).
[14] J. S. Briggs and V. Schmidt, J. Phys. B: At., Mol. Opt. Phys. **33**, R1 (2000).
[15] B. Krässig, S. J. Schaphorst, O. Schwarzkopf, N. Scherer, and V. Schmidt, J. Phys. B: At., Mol. Opt. Phys. **29**, 4255 (1996).
[16] M. Gisselbrecht, M. Lavollee, A. Huetz, P. Bolognesi, L. Avaldi, D. P. Seccombe, and T. J. Reddish, Phys. Rev. Lett. **96**, 153002 (2006).
[17] T. Weber, A. Czasch, O. Jagutzki, A. Müller, V. Mergel, A. Kheifets, J. Feagin, E. Rotenberg, G. Meigs, M. H. Prior, S. Daveau, A. L. Landers, C. L. Cocke, T. Osipov, H. Schmidt-Böcking, and R. Dörner, Phys. Rev. Lett. **92**, 163001 (2004).
[18] H. Ni, S. Chen, C. Ruiz, and A. Becker, J. Phys. B: At., Mol. Opt. Phys. **44**, 175601 (2011).
[19] A. Knapp, A. Kheifets, I. Bray, T. Weber, A. L. Landers, S. Schössler, T. Jahnke, J. Nickles, S. Kammer, O. Jagutzki, L. P. H. Schmidt, T. Osipov, J. Rösch, M. H. Prior, H. Schmidt-Böcking, C. L. Cocke, and R. Dörner, Phys. Rev. Lett. **89**, 033004 (2002).
[20] A. Liu and U. Thumm, Phys. Rev. Lett. **115**, 183002 (2015).
[21] A. Becker and F. H. M. Faisal, Phys. Rev. A **50**, 3256 (1994).
[22] A. Becker and F. H. M. Faisal, J. Phys. B: At., Mol. Opt. Phys. **38**, R1 (2005).
[23] G. M. Pindzola, M. S. Laurent, and J. P. Colgan, J. Phys. B: At., Mol. Opt. Phys. **50**, 185601 (2017).
[24] R. Dörner, J. M. Feagin, C. L. Cocke, H. Bräuning, O. Jagutzki, M. Jung, E. P. Kanter, H. Khemliche, S. Kravis, V. Mergel, M. H. Prior, H. Schmidt-Böcking, L. Spielberger, J. Ullrich, M. Unversagt, and T. Vogt, Phys. Rev. Lett. **77**, 1024 (1996).
[25] M. Kurka, J. Feist, D. A. Horner, A. Rudenko, J. Y. H., K. U. Kühnel, L. Foucar, T. N. Rescigno, C. W. McCurdy, R. Pazourek, S. Nagele, M. Schulz, O. Herrwerth, M. Lezius, M. F. Kling, M. Schöffler, A. Belkacem, S. Düsterer, R. Treusch, B. I. Schneider, L. A. Collins, J. Burgdörfer, C. D. Schröter, R. Moshammer, and J. Ullrich, New J. Phys. **12**, 073035 (2010).
[26] H. Bräuning, R. Dörner, C. L. Cocke, M. H. Prior, B. Krässig, A. S. Kheifets, I. Bray, A. Bräuning-Demian, K. Carnes, S. Dreuil, V. Mergel, P. Richard, J. Ullrich, and H. Schmidt-Böcking, J. Phys. B: At., Mol. Opt. Phys. **31**, 5149 (1998).
[27] J. Ullrich, R. Moshammer, A. Dorn, R. Dörner, L. P. H. Schmidt, and H. Schmidt-Böcking, Rep. Prog. Phys. **66**, 1463 (2003).
[28] O. Jagutzki, A. Cerezo, A. Czasch, R. Dörner, M. Hattass, V. Mergel, U. Spillmann, K. Ullmann-Pfleger, T. Weber, H. Schmidt-Böcking, and G. D. W. Smith, IEEE Trans. Nucl. Sci. **49**, 2477 (2002).
[29] W. Zhang, H. Li, K. Lin, P. Lu, X. Gong, Q. Song, Q. Ji, J. Ma, H. Li, H. Zeng, F. He, and J. Wu, Phys. Rev. A **96**, 033405 (2017).